DOI: 10.1002/adfm.200500737

Mesostructured Silica Chemically Doped with Ru^{II} as a Superior Optical Oxygen Sensor**

By *Bingfu Lei*, *Bin Li*,* *Haoran Zhang*, *Shaozhe Lu*, *Zhuhong Zheng*, *Wenlian Li*, and *Yue Wang*

Novel oxygen sensors consisting of a $[Ru(bpy)_2phen]^{2+}$ (bpy: 2,2′-bipyridyl, phen: phenathroline) portion covalently grafted to a mesostructured silica-based network are prepared in situ via a sol–gel approach with the help of cetyltrimethylammonium-bromide (CTAB) surfactant. 1,10-Phenanthroline covalently grafted to 3-(triethoxysilyl)propyl isocyanate is used as not only the sol–gel precursor but also as the second ligand of the $Ru(bpy)_2Cl_2 \cdot 2H_2O$ complex to prepare the sol–gel-derived mesostructured silicates for an oxygen sensor. For comparison purposes, the oxygen sensors in which $[Ru(bpy)_2phen]Cl_2$ is conventionally physically incorporated into the matrix are also prepared. Elemental analysis, NMR, Fourier transform IR, UV-vis electronic absorption, luminescence-intensity quenching Stern–Volmer plots, and excited-state decay analysis are used to characterize the obtained oxygen sensors. These obtained bulk xerogels and spin-coated thin films show that the homogeneity and the sensitivity of the covalently grafted samples are superior to those of the physically incorporated ones, and the highest sensitivity is obtained in the mesostructured bulk xerogel. This improvement in oxygen sensitivity is attributed to the increased diffusivity of oxygen in the uniform and nearly parallel porous structure of the Mobil Catalytic Material 41 mesostructured matrix, the enhanced homogeneity results from the covalently grafted propyl group in $–Si–(CH_2)_3–$ that acts as the fundamental spacer which prevents interaction between the attached Ru^{II} complex and the silica matrix, and optimal dispersion in the mesopores during the sol–gel polycondensation. Furthermore, the greatly minimized leaching effect of the sensing molecules could be observed in the covalently grafted system. The covalent grafting strategy presented in this paper provides superior optical oxygen sensors with homogeneous distribution, improved sensitivity, and simplified calibration plots.

1. Introduction

The determination of oxygen concentration in gaseous samples, aqueous samples, and biological fluids has important ramifications in medicinal, environmental, and analytical chemistry. Traditionally, O_2 is quantified by using a Clark-type amperometric electrode, which is based on the electroreduction of O_2 on a polarized cathode.[1] However, the traditional Clark electrode suffers from several drawbacks, such as oxygen consumption during the sensing process, relatively long response times, and the tendency of the electrode to be poisoned by sample constituents (e.g., H_2S, proteins, and certain anesthetics). Given these limitations, the search for novel optically based O_2 sensors to replace the older electrochemical methods is a major goal of current analytical science.

Tremendous efforts over the past two decades have been devoted to the design of novel high-performance (high sensitivity, long-term stability, and good linear calibration plots) optical oxygen sensors.[2–34] For optical oxygen sensors, a particularly attractive method is based on the luminescence quenching of a luminophore by the presence of oxygen because oxygen is a powerful quencher of the electronically excited state of a dye molecule. The excited-state lifetime and/or emission intensity of the luminophore decreases as the oxygen concentration increases. Either of these changes can be quantified and provide the basis for a relatively simple, inexpensive analysis method. In homogeneous media with a single-exponential decay, oxygen quenching of the intensity and lifetime of this kind of oxygen sensor is described by the Stern–Volmer equation:[28]

$$I_0/I = \tau_0/\tau = 1 + K_{SV} p_{O_2} = 1 + \kappa \tau_0 p_{O_2} \quad (1)$$

where I and τ are the luminescence intensity and excited-state lifetime of the luminophore, respectively, the subscript 0 denotes the absence of oxygen, K_{SV} is the Stern–Volmer constant, κ is the bimolecular quenching constant, and p_{O_2} is the partial pressure of oxygen at 1 atm (1 atm = 101 325 Pa) pressure. A plot of I_0/I or τ_0/τ versus oxygen concentration should give a straight-line relationship with slope K_{SV}, and an intercept of

[*] Prof. B. Li, Dr. B. Lei, H. Zhang, Prof. S. Lu, Prof. Z. Zheng, Prof. W. Li
Key Laboratory of Excited State Processes
Changchun Institute of Optics Fine Mechanics and Physics, and Graduate School of the Chinese Academy of Sciences
Chinese Academy of Sciences
Changchun 130033 (P.R. China)
E-mail: lib020@ciomp.ac.cn
Prof. Y. Wang
Key Laboratory for Supramolecular Structure and Materials of Ministry of Education
Jilin University
Changchun 130012 (P.R. China)

[**] The authors gratefully thank the financial supports of the One Hundred Talents Project from the Chinese Academy of Sciences and the National Natural Science Foundations of China (Grant No. 20571071).

one on the vertical axis. The lifetime decay of the luminophore in homogeneous media can be described by a single-exponential equation:[6,22]

$$I(t) = \alpha \exp(-t/\tau) \quad (2)$$

where $I(t)$ is the luminescence intensity at time t, and α is the pre-exponential factor.

Many luminescent dyes have been tested as oxygen-sensing probes. Among them, luminescent transition metal complexes, particularly those of ruthenium(II) polypyridyl compounds, have been frequently utilized as the most useful oxygen-sensitive dyes owing to their highly emissive metal-to-ligand charge-transfer (MLCT) state, long fluorescence lifetime, large Stokes shift, high photochemical stability, high sensitivity to oxygen, and strong visible absorption in the blue–green region of the electromagnetic spectrum. The quenching process of Ru^{II} by O_2 can be described as follows: $Ru^{II}* + O_2 \rightarrow Ru^{II} + O_2*$, where Ru^{II} denotes the complex and "*" is the excited state. Virtually all complexes used as sensing probes should be supported on an inorganic or organic polymer matrix. Indeed, the support may have quite stringent criteria for suitable performance. For example, in an oxygen sensor, a high diffusion coefficient is necessary for a rapid response; a highly locally effective quenching around the oxygen probe is necessary for good sensitivity, and considerable interest in physiological monitoring necessitates a high degree of biocompatibility.[11] In addition, the sensor support must lend itself to convenient and robust attachment to the sensor probe.

Sol–gel-derived materials are ideal supports to be used to immobilize dyes for application in optical chemical sensors owing to their suitable chemical and photochemical stability and their optical properties. They can also be made into usable forms such as thin films and bulk pieces.[22–24,28–33,35–39] In general, a sol–gel process begins with the formation of a colloidal suspension of the reaction products called a sol, usually from metal alkoxide monomers through hydrolysis and polycondensation reactions at room temperature. The sol undergoes a transition to a soft porous wet gel, which eventually becomes a solid porous aggregate of extremely small particles known as a xerogel. Using organosilicon compounds as the reactants under certain conditions, the xerogel may eventually become a porous transparent silica-gel glass provided that the silica particles are small enough compared to the light wavelengths. It seems worthy, therefore, to use this kind of support for oxygen sensors. So far, many ruthenium(II) complexes have been reported to be successfully incorporated into inorganic oxide thin films as well as in oxide bulk gels, and applications in optical sensors have also been demonstrated.[4,22–24,27–29,32,38] However, the sol–gel-derived oxygen sensors are frequently heterogeneous on a microscopic scale when the ruthenium(II) complexes are physically incorporated.[6,11,16,19,22,24,40] This microheterogeneity gives rise to complex and poorly characterized decay kinetics, and this complexity may result in obscure sensor responses and nonlinear Stern–Volmer quenching curves. In addition, the leaching of the dopants into the analyte solution is usually encountered when the dopant molecules are weakly physically adsorbed within the sol–gel cages surface, and this represents a serious problem in terms of signal stability and longevity.[28]

Covalent grafting of the dopant to the backbone of silica networks via the $Si–CH_2$ bond can overcome the above-mentioned problems.[41–47] In our present work, we use the modified 1,10-phenathroline compound (denoted as phen-Si, the chemical structure is depicted in Scheme 1) as the second ligand of the $Ru(bpy)_2Cl_2$ (bpy = 2,2′-bipyridyl) complex and as a precursor of the sol–gel process to realize the covalent grafting of the

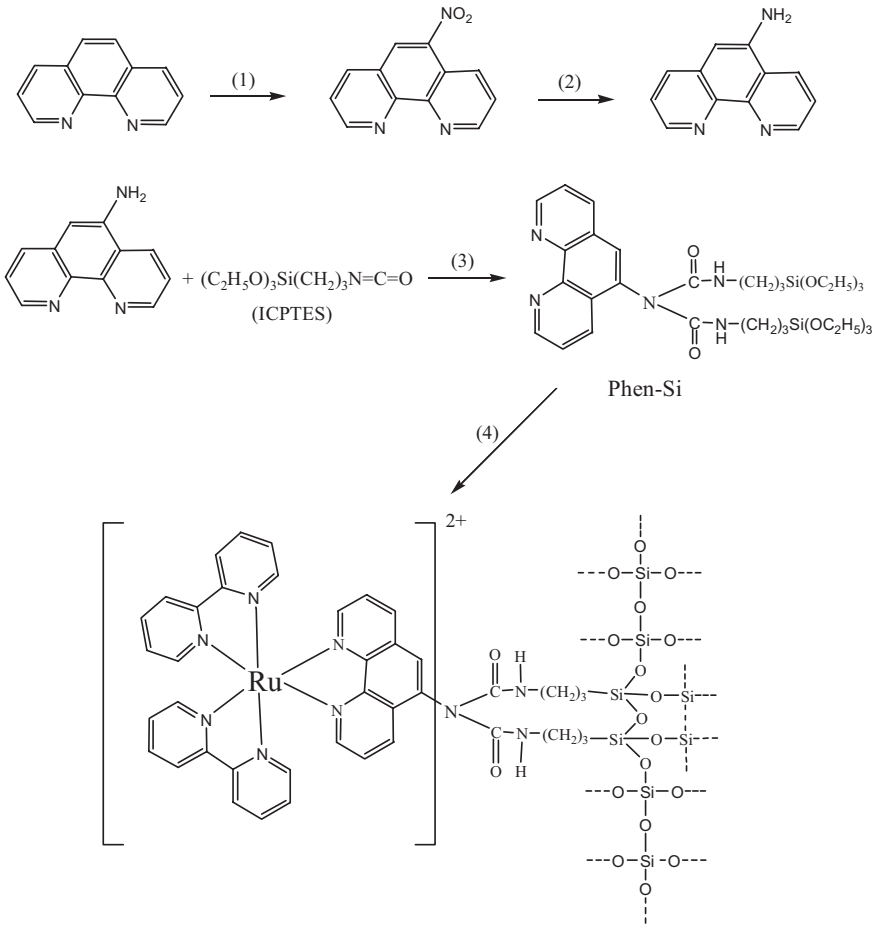

Scheme 1. Synthesis of the hydrolyzable phen-Si ligand, and preparation of the $[Ru(bpy)_2phen]^{2+}$ covalently grafted mesostructured silicates produced in situ via a sol–gel approach. Reagents and experimental conditions: 1) HNO_3/H_2SO_4, 160–170 °C, 2 h; 2) hydrazine monohydrate, Pd/C 5 %, ethanol; 3) $CHCl_3$, 80 °C, overnight; 4) TEOS, H_2O, HCl, ethanol, $Ru(bpy)_2Cl_2$.

ADVANCED FUNCTIONAL MATERIALS

$[Ru(bpy)_2phen]^{2+}$ portion to the backbone of the silicates via in situ hydrolysis and condensation in the presence of the complex $Ru(bpy)_2Cl_2$ and tetraethoxysilane (TEOS) under acidic catalytic conditions. Using this strategy, we have successfully obtained crack-free and transparent covalently grafted 1,10-phenathroline functionalized silicates (thin films and bulk xerogels) for oxygen sensors. At the same time, the sol–gel-derived samples were also prepared as mesostructures using the cetyltrimethylammoniumbromide (CTAB) template-directed method.[48–51] The sensitivity properties of our present oxygen-sensor samples were discussed based on the luminescence intensity quenching. Changes in the sensitivity, Stern–Volmer plots, and excited-state decays of these samples were also discussed. The addition of phen-Si results in a more homogeneous and well-defined distribution of the Ru^{II} complex in the samples, giving rise to better linear calibration plots.

2. Results and Discussion

By using the phen-Si compound we have succeeded in covalently grafting the $[Ru(bpy)_2phen]^{2+}$ portion to the mesostructured silicates produced in situ via a sol–gel approach for oxygen sensors. The synthesis procedure of this material is outlined in Scheme 1.

Successful covalent grafting of 3-(triethoxysilyl)-propyl isocyanate (ICPTES) to silicates can be supported by the Fourier transform IR (FT-IR) spectrum.[47,52] Patterns (A), (B), and (C) of Figure 1 show the FT-IR spectra of the modified ligand phen-Si, the covalently grafted monomer, and the physically

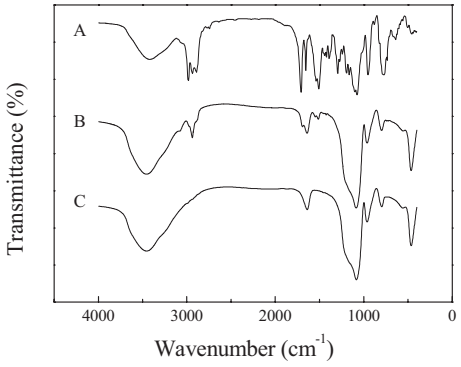

Figure 1. IR spectra for phen-Si (A), a covalently grafted monomer (B), and a physically incorporated monomer (C).

incorporated monomer, respectively. In Figure 1A, the spectrum of phen-Si is dominated by the ν_{as}(Si–CH_2, 1196 cm^{-1}) and ν_{as}(Si–OEt, 1079 cm^{-1}) absorption bands, characteristic of hydrolyzable trialkoxylsilyl functions. In Figure 1B, the peaks at 1690, 1554, and 1517 cm^{-1} are the absorption of the urea groups (NH–CO–NH) from phen-Si. The location and their assignments for other absorption peaks are 2979 (ν_{as}, CH_2), 2927 (ν_s, CH_2), and 1500 (δ, CH_2). The absorption band at 1085 cm^{-1} (ν_{as}, Si–O–Si) substantiates the formation of a silica framework. In addition, the peak at 1690 cm^{-1} in the covalently grafted monomer shows an obvious red-shift ($\Delta\nu = 18$ cm^{-1}) compared to 1708 cm^{-1} for free phen-Si. The complexation between $Ru(bpy)_2Cl_2$ and the phen-Si ligand leads to a decrease in their vibration frequencies, resulting in a red-shift of the spectra.

The luminescence spectra of mesostructured sol–gel-derived monomer are shown in Figure 2. The spectra of complex $[Ru(bpy)_2phen]Cl_2$ dissolved in anhydrous ethanol are also given for comparison. The absorption spectrum of $[Ru(bpy)_2phen]Cl_2$ shows an intense absorption band at 457 nm and a shoulder at 425 nm, which are both assigned to the MLCT ($t_{2g}(Ru) \rightarrow \pi^*(bpy)$) transition. The emission maxima observed at 580–605 nm arises from ligand-to-metal charge-transfer excited states.[6] As shown in Figure 2, the absorption feature of $[Ru(bpy)_2phen]^{2+}$ entrapped within the TEOS sol–gel thin film is not significantly different from that observed in ethanol. The emission maximum wavelength, however, showed a blue-shift of approximately 14 nm, from 602 to 588 nm, when the complex was immobilized within the solid matrix. This fact can be explained by the mechanism of so-called "rigidochromism", which was originally termed by Wrighton and Morse[53] and has been discussed by others.[32,38,54,55] Rigidochromism arises because the excited state of the complex is an energetically unfavorable configuration on initial excitation. In fluid media, the unrelaxed Franck–Condon excited state can thermally relax to its energetically most-stable configuration by the surrounding solvent dipoles, and gets the lowest energy emission from a relaxed excited state. As the media stiffens, that is, when the surrounding media experiences sol-to-gel conversion, the excited state cannot relax within its lifetime and the emission is from the higher-energy unequilibrated state, which results in a blue-shift in the emission. The thin film possesses similar characteristics in the luminescence spectra to that of the bulk monomer.

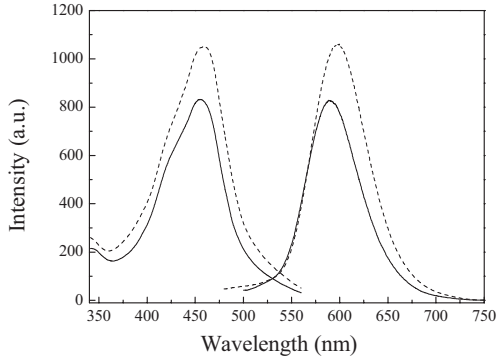

Figure 2. Absorption (left) and emission (right) spectra of sol–gel-derived mesostructured monomer oxygen sensor (solid lines) and complex $[Ru(bpy)_2phen]Cl_2$ in anhydrous ethanol (dashed lines).

The performance of an oxygen sensor depends on the structure of the support to a great extent. For example, a high gas-

diffusion coefficient is necessary for rapid response; a high locally effective quenching around the complex molecule is necessary for good sensitivity. The discovery of periodic mesoporous inorganic materials known as Mobil Catalytic Material 41 (MCM-41) characterized by a large surface area and narrow pore size distribution has opened up new opportunities for confining close-packed, functionalized molecules within parallel-aligned porous channels. The covalent grafting of complex molecules into ordered porous MCM-type materials is of importance in a number of areas and a number of interesting electronic and optical properties have been observed in the MCM-41 system.[49,56] The MCM-41 matrix is expected to be an effective support for preparation of oxygen sensors with excellent performance because of its uniform and nearly parallel porous structure. We previously demonstrated a method to prepare the surfactant ruthenium(II) complexes that is used to synthesize mesostructured materials with a regular, hexagonal array of variable-pore-size uniform channels.[57] In this study, the oxygen sensor was prepared as mesostructured using the CTAB surfactant template.[48–51] Figure 3 shows the small-angle X-ray diffraction (SAXRD) patterns of the surfactant-extracted mesostructured thin film and bulk sample. Both the thin film and bulk samples show three intense broad Bragg reflections that can be indexed as d_{100}, d_{110}, and d_{200}, which are characteristic of a highly ordered hexagonal mesostructure. The presence of these three diffraction peaks indicates that both the thin film and bulk samples have MCM-41-type architecture with long-range order. Acid extraction of the CTAB surfactant template from both samples was achieved without loss of the hexagonally ordered structure. The value of a_0 for bulk xerogel obtained from the SAXRD pattern ($a_0 = 2\,d_{100}/\sqrt{3}$) is higher than that of the thin film, 4.49 and 4.42 nm, respectively. Such difference is similar to that reported by Li et al.[49]

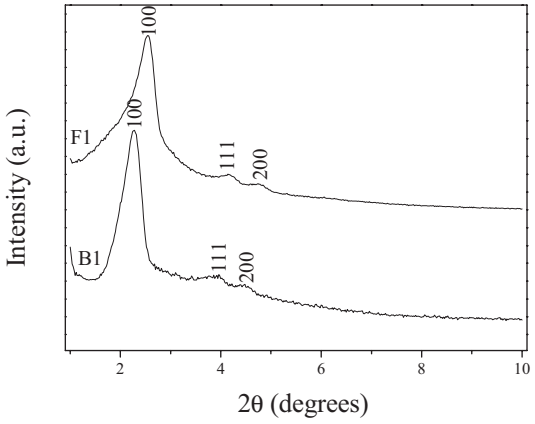

Figure 3. SAXRD diffraction patterns of the surfactant-extracted sol–gel-derived mesostructured thin film (F1) and the mesostructured bulk sample (B1).

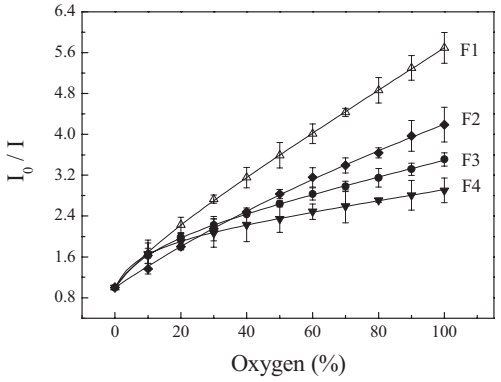

Figure 4. Typical luminescence intensity-based Stern–Volmer plots for the sol–gel-derived thin films. F1: a covalently grafted mesostructured thin film; F2: a covalently grafted amorphous thin film; F3: a physically incorporated mesostructured thin film; and F4: a physically incorporated amorphous thin film. The solid lines represent the best fit using the two-site model.

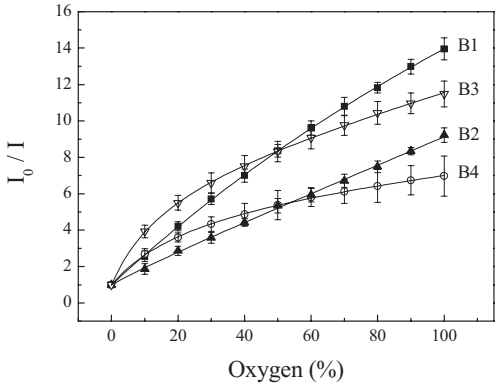

Figure 5. Typical luminescence intensity-based Stern–Volmer plots for the bulk xerogel. B1: a covalently grafted mesostructured bulk xerogel; B2: a covalently grafted amorphous bulk xerogel; B3: a physically incorporated mesostructured bulk xerogel; and B4: a physically incorporated amorphous bulk xerogel. The solid lines represent the best fit using the two-site model.

Figures 4 and 5 present the typical intensity-based Stern–Volmer plots for a randomly selected series of two-month-old Ru^{II}-doped thin films and bulk xerogels, respectively. The intensity-based Stern–Volmer oxygen-quenching fitting parameters are also tabulated in Table 1. Inspection of these results reveals several key points. Firstly, obvious downward curvature is exhibited in both the physically incorporated amorphous samples (bulk xerogel and the thin film) without the Si–CH_2 covalent bond. The origin of this nonlinearity is associated with the luminophore molecules which are distributed simultaneously between two or more sites within the sol–gel-derived silicate in which one site is more heavily quenched than the other. Consequently, the microheterogenous sites exhibit different quenching constants K_{SV} and unquenched lifetime τ_0 values. Several models have been developed to help explain these results as previously discussed by Demas and co-workers[4,6,11,40] and others.[16,22,34,35] In microheterogenous solid-based oxygen sensors, a two-site model has been found to have excellent ability

ADVANCED FUNCTIONAL MATERIALS

Table 1. Intensity-based Stern–Volmer oxygen-quenching fitting parameters for Ru^{II}-doped bulk xerogels and thin films.

Samples	I_0/I_{100}	Stern–Volmer model		Two-site model [b]			
		K_{SV} ($O_2\%^{-1}$)	r^2 [a]	K_{SV1}($O_2\%^{-1}$)	K_{SV2}($O_2\%^{-1}$)	f_{01} [c]	r^2
F1	5.81	0.0490±0.0008	0.9877	0.1249±0.0062	0.0188±0.0009	0.69±0.04	0.9999
F2	4.28	0.0338±0.0006	0.9879	0.0473±0.0023	0.0017±0.0001	0.91±0.03	0.9994
F3	3.52			0.1681±0.0084	0.0068±0.0003	0.57±0.01	0.9998
F4	2.92			0.2489±0.0124	0.0049±0.0002	0.82±0.01	0.9997
B1	14.31	0.1369±0.0023	0.9890	0.0290±0.0014	0.2695±0.0135	0.16±0.02	0.9985
B2	9.25	0.0825±0.0006	0.9979	0.3102±0.0155	0.0581±0.0029	0.32±0.06	0.9992
B3	11.5			0.0061±0.0003	0.4811±0.0241	0.11±0.01	0.9998
B4	7.02			0.0067±0.0003	0.3560±0.0179	0.16±0.01	0.9975

[a] Samples were aged for two months, and when an entry is not given, the Stern–Volmer model is the best model for the fitting. [b] Terms are from Equation 3. [c] $f_{01}+f_{02}=1$.

to fit the experiment data.[16,22,24,58] In this model, the straight-line intensity Stern–Volmer equation then becomes

$$\frac{I_0}{I}=\frac{1}{\frac{f_{01}}{1+K_{SV1}p_{O_2}}+\frac{f_{02}}{1+K_{SV2}p_{O_2}}} \tag{3}$$

where f_{0i} values are the fraction of each of the two sites contributing to the unquenched intensity, K_{SVi} values are the associated Stern–Volmer quenching constants for the two sites, and p_{O_2} is the partial pressure of oxygen at 1 atm pressure. In this case, there are two lifetime components, and the excited lifetime decay analysis may be described by

$$I(t)=\alpha_1\exp(-t/\tau_1)+\alpha_2\exp(-t/\tau_2) \tag{4}$$

where $I(t)$ represents the fluorescence intensity at time t, the subscripts 1 and 2 denote the assigned lifetime components, and α_i denotes the pre-exponential factors. The weighted mean lifetime τ_m can be calculated by using the following equation:[22]

$$\langle\tau_m\rangle=\sum_{i=1}^{2}\alpha_i\tau_i/\sum_{i=1}^{2}\alpha_i \tag{5}$$

Secondly, all the four covalently grafted bulk xerogels and thin films show greatly enhanced linear oxygen-quenching plots. A linear calibration Stern–Volmer plot of an oxygen sensor is very important because it is easy to calibrate and does not require a multipoint calibration strategy when exposed to practical application. As is shown in these figures, the Stern–Volmer oxygen-quenching plots of these covalently grafted samples appear to deviate very little from single-exponential plots, especially at low O_2 concentrations, and they appear more nearly linear. The downward curvature of the Stern–Volmer plots are fully in line with the behavior of a wide variety of luminophore-doped sol–gel-derived xerogels,[11,16,22,24,40,58] and this kind of downward curvature plot necessitates a model more complex than a single-species quenched bimolecularly. It is worth noting that the Demas two-site model[6] is enough to fit the intensity-quenching curves of all these samples. It is not surprising given the well-known ability of two exponentials to give excellent fits to complex decay curves, which are made up of distribution functions of exponential decays, especially at the count levels used on most single-photon counting instruments. All these results demonstrate that the microenvironment that surrounds the Ru^{II} molecules changes from being heterogeneous within the physically incorporated samples to being more homogeneous within the covalently grafted samples.

The third feature observed from the Stern–Volmer plots is that the sensitivities of the covalently grafted samples are higher than those of the physically incorporated ones over the oxygen concentration range examined, and the greatest sensitivity is seen from the mesostructured bulk sample. The higher K_{SV} values in the covalently grafted mesostructured samples compared to those in the covalently grafted amorphous samples indicate that the luminophore is more easily quenched by oxygen. This result can be attributed to the uniform and nearly parallel porous structure of the MCM-41 support with large surface areas and narrow pore size distributions. The luminophore confined within the MCM-41 highly ordered parallel-aligned porous channels have a higher locally effective quenching by O_2, resulting in increased sensitivity. Therefore, the Ru^{II} complex covalently grafted to the network of the modified silicates are located on sites characterized by a higher diffusion rate that enhances luminescence quenching by oxygen in these regions. Additionally, in comparison to the xerogel samples, the spin-coated films have lower f_{01} values.

Finally, inspection of these figures shows that the error bars (obtained from triplet samples prepared under the same conditions) associated with the physically incorporated samples are larger in comparison to the covalently grafted samples. This result demonstrates that the sample-to-sample reproducibility is better for the covalently grafted samples.

The aforementioned data reveal that improved sensitivity and more nearly linear Stern–Volmer plots can be obtained by the covalent grafting strategy. We attribute these results to the covalently grafted Si–CH_2 bond and the highly ordered parallel-aligned porous channels of the support (MCM-41). This assumption can be further proved by the time-resolved intensity-decay experiments. It has been reported that if the time-re-

solved intensity decays appear as single exponential, the binding sites of the Ru^{2+} complexes are distributed homogeneously within the silicates support.[24]

Figure 6 presents the time-resolved intensity-decay curves of four-month-old Ru^{II}-doped bulk samples. The fitting parameters of these decay curves are summarized in Table 2. These results clearly show that the time-resolved intensity decay of the physically incorporated xerogel is at least double exponential. This is a common behavior for a luminophore doped in a wide variety of host matrixes.[16,24,38,40,58,59] When the Ru^{II} complex is covalently grafted to the silicates network, the time-resolved intensity decay traces change from double exponential to single exponential, resulting in near single-exponential intensity decay curves and linear Stern–Volmer plots (as shown in Figs. 4 and 5). These results are similar to those previously reported by Bright and co-workers.[24] The result of the time-resolved decay curves is consistent with the Stern–Volmer plots (as shown in Fig. 5). All these data further indicate that the Ru^{II} molecules are distributed more homogeneously within the covalently grafted samples.

Figure 7 shows the typical dynamic response of the covalently grafted mesostructured bulk sample on exposure to pure N_2 and O_2 atmospheres which was varied periodically. From these time-dependent measurements, the 95 % response ($t_{95\downarrow}$) and 95 % recovery ($t_{95\uparrow}$) times to an alternating atmosphere of pure N_2 and O_2 can be calculated. These values are defined as the time taken for a sample to attain 95 % of its total emission intensity change when the gas is changed from pure N_2 to pure O_2 and from pure O_2 to pure N_2, respectively. The covalently grafted mesostructured bulk sample exhibits a fully reversible response with response ($t_{95\downarrow}$) and recovery ($t_{95\uparrow}$) values of 4 and ca. 10 s, respectively. The obvious difference in the response times can be explained by the mathematical expressions developed elsewhere by Mills and Chang and Mills and Lepre to describe the diffusion-controlled dynamic response and recovery behavior of a hyperbolic-type sensor to changing ana-

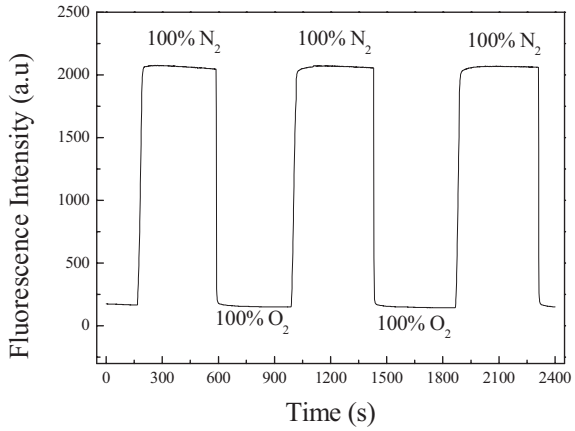

Figure 7. Relative luminescence intensity of the 588 nm emission as a function of time for a typical covalently grafted $[Ru(bpy)_2phen]^{2+}$ mesostructured bulk sample subjected to an atmosphere which was varied periodically between pure N_2 and pure O_2.

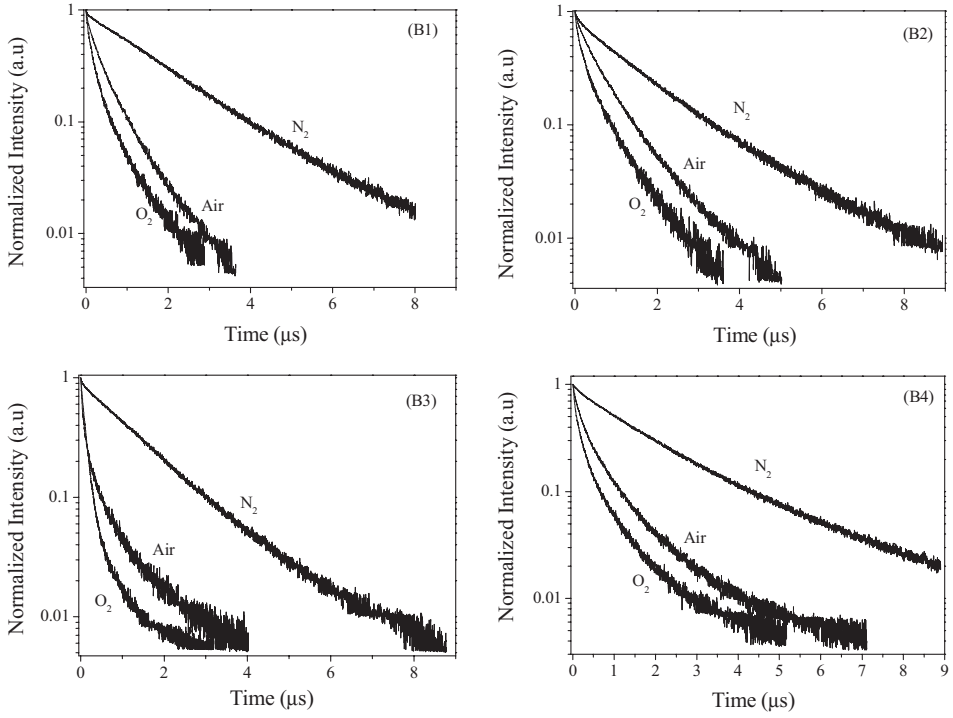

Figure 6. Typical time-resolved intensity decay curves of four-month-old Ru^{II}-doped bulk samples. B1: a covalently grafted mesostructured bulk xerogel; B2: a covalently grafted amorphous bulk xerogel; B3: a physically incorporated mesostructured bulk xerogel; and B4: a physically incorporated amorphous bulk xerogel.

ADVANCED FUNCTIONAL MATERIALS

Table 2. Time-resolved intensity decay constants for Ru^{II}-doped bulk xerogel samples [a,b].

Sample	Gas	a_1	τ_1	a_2 [a]	τ_2 [b]	$<\tau>$ [a,b]	r^2
B1	N_2	0.92±0.02	1.766±0.001				0.9995
	Air	0.50±0.04	0.571±0.002	0.36±0.01	0.134±0.002	0.387	0.9994
	O_2	0.27±0.02	0.208±0.004	0.77±0.02	0.098±0.005	0.127	0.9987
B2	N_2	0.79±0.01	1.754±0.002	0.13±0.01	0.217±0.003	1.535	0.9996
	Air	0.61±0.02	0.669±0.002	0.29±0.01	0.178±0.003	0.511	0.9993
	O_2	0.46±0.02	0.230±0.002	0.48±0.02	0.112±0.004	0.169	0.9983
B3	N_2	0.82±0.05	1.275±0.003	0.12±0.02	2.123±0.004	1.383	0.9996
	Air	0.24±0.02	0.637±0.005	0.70±0.04	0.091±0.009	0.228	0.9918
	O_2	0.12±0.02	0.309±0.001	0.84±0.01	0.097±0.003	0.123	0.9995
B4	N_2	0.83±0.01	1.871±0.002	0.12±0.01	0.332±0.003	1.673	0.9997
	Air	0.44±0.01	0.759±0.002	0.52±0.01	0.146±0.001	0.428	0.9992
	O_2	0.35±0.03	0.511±0.008	0.61±0.04	0.083±0.005	0.241	0.9981

[a] When an entry is not given, the single-exponential model is good enough for the fitting. The values of thin films spin-coated on the sodalime silicate glass were not available due to the intrinsic emission of the sodalime silicate glass support. [b] Terms are from Equation (5).

lyte concentration.[60,61] From Figure 7, we can see that the sensor response is stable and very rapid. We attribute the fast response to the fact that the covalently grafted $Si–CH_2$ bond and the highly ordered channels of the mesoporous support facilitates the high diffusion of gas. Furthermore, stable and reproducible signals under 457 nm light irradiation can be obtained from the covalently grafted samples (bulk and thin film), while the physically incorporated samples show drifted intensities (not shown in Fig. 7), indicating that the covalently grafted samples are more stable due to the $Si–CH_2$ covalent bond compared to the physically incorporated samples.

Sensitivity and stability over time are two key analytical characters of merit for any sensor.[24] We have measured the average sensitivity and response stability of the covalently grafted mesostructured bulk over four months every 15 days, and the result reveals that the effect of aging time on the O_2 sensor's average sensitivity and response stability is small enough to be neglected. The relative standard deviation for the sensitivity (I_0/I) was 1.8 %. However, the sensitivity of the amorphous physically incorporated sample drifts with time over four months due to the intrinsic microheterogeneity of the sol–gel-derived silicates. This type of behavior has been reported previously.[8,24] We speculate that the observed improvements in sensor long-term stability and sustained high sensitivity arise from the increased flexibility that overcomes the xerogel shrinkage and pores collapse with time due to the $Si–CH_2$ covalent bond.[24]

Dissolved-oxygen sensing is of great importance in environmental, industrial, and medical applications. One fundamental but crucial question that remains when this kind of covalently grafted oxygen sensor is used for the dissolved-oxygen detection is whether the luminophore leaches into the liquid phase. For this consideration, complex-leaching experiments were performed for both the surfactant-extracted covalently grafted mesostructured and physically incorporated amorphous bulk samples by soaking them in a dimethylformamide (DMF) solution at 60 °C in a sealed cuvette under magnetic stirring, as described previously.[47] The complex-leaching investigations have revealed that a greatly minimized leaching effect can be observed for the sol–gel-derived mesostructured bulk sample incorporating the covalently grafted Ru^{II} complex, in comparison to a similar bulk sample incorporating the physically entrapped Ru^{II} complex. The mesostructured covalently grafted xerogel retains most of its activity (95 %), whereas the physically entrapped xerogel shows a 60 % reduction in sensitivity that is due to the leaching of the entrapped dopants. This result reveals that the covalent bond between the complex and the sol–gel matrix can effectively prevent the leaching of dopants, which is in excellent agreement with the result reported by Li et al.[47] The large minimization of the leaching is a crucial aspect for the dissolved-oxygen sensor applications. Work is currently underway in our laboratory to fully characterize the dissolved-oxygen sensing properties.

3. Conclusions

We have demonstrated that covalently grafted Ru^{II} complex mesostructured bulk xerogels and thin films are suitable candidates for an optical oxygen sensor compared to conventional physically incorporated xerogels. As expected, a remarkable increase in homogeneity has been realized by covalently grafting the organometallic Ru^{II} complex to the inorganic network during the sol–gel process using the in situ approach. The response time is short, due to the mesoporosity of the MCM-41 system. The greatly minimized leaching effect of the sensing molecule can be observed in the covalently grafted samples. Furthermore, the covalent $Si–CH_2$ bond allows us to extend this kind of sensor for use in dissolved-oxygen detection, which is more important in practical applications. Our results suggest that it should be possible to covalently graft the Ru^{II} complex onto mesophase silica for oxygen-sensor applications, and corresponding mesostructured oxygen sensors show superior properties to those of amorphous samples. Uniformity, improved sensitivity, and simplified calibration sensors can be also obtained using the covalent grafting strategy.

4. Experimental

Chemical Reagents: The ICPTES and the 5% Pd/C catalyst were purchased from Aldrich (Milwaukee, WI, USA) and used as received. Anhydrous $RuCl_3$ (99.99%) was obtained from Acros Organics (Geel, Belgium). The complex bis(2,2′-bipyridyl) ruthenium(II) chloride dihydrate, $Ru(bpy)_2Cl_2 \cdot 2H_2O$, was synthesized and purified as described in the literature [62]. Concentrated HCl, DMF, TEOS, and EtOH were obtained from Beijing Chemical Company. The water used in our present work was deionized. The solvent, DMF, was used after distillation in a vacuum.

Preparation of phen-Si: The phen-Si was prepared using 5-amino-1,10-phenanthroline (phen-NH_2) and ICPTES as the starting material. The synthesis of phen-NH_2 was performed by nitration of 1,10-phenanthroline in a mixture of concentrated sulfuric acid and fuming nitric acid, followed by reduction of the nitro derivative with hydrazine over a 5% Pd/C catalyst. The detailed synthetic procedure of phen-Si has been described in detail elsewhere [63–65]: phen-NH_2 (0.200 g; 1.02 mmol) was dissolved in 20 mL chloroform and excess ICPTES (1.7 mL; 6.37 mmol) was added while the solution was stirred. The excessive chloroform was removed by evaporation at atmospheric pressure, and the residual mixture was heated at 80 °C in a covered flask for 12 h. Cold hexane was added to precipitate a yellow-white precipitate from the mixture. The final filtered-off precipitate was washed with several portions of cold hexane and then was purified in methanol, and dried in vacuo. Elemental analysis for phen-Si ($C_{32}H_{51}N_5O_8Si_2$): Calculated: C, 55.71; H, 7.45; N, 10.15%. Found C, 55.6; H, 7.30; N, 10.4%. NMR ($CDCl_3$): δ 0.52 (m, 4H), 1.13 (t, 18 H), 1.60 (m, 4H), 3.21 (m, 4H), 3.69 (q, 12 H), 7.25 (s, 1H), 7.16 (s, 1H), 7.68 (m, 2H), 7.87 (s, 1H), 8.24 (m, 2H), 9.23 ppm (m, 2 H). IR (KBr, cm^{-1}): NH stretch (3270 cm^{-1}), NH–CO–NH stretch (1690, 1554, and 1517 cm^{-1}), Si–CH_2 (1196 cm^{-1}).

Sample Preparation: The in situ process had been proved to be an excellent approach to incorporate the organometallic complex into various sol–gel hosts [41,42,47,49]. The present work has the purpose of preparing mesostructured silicates with a covalently grafted Ru^{II} complex produced in situ via a sol–gel approach for oxygen sensor. An important point that needs to be pointed out in our system is that careful optimization of the processing conditions is necessary to obtain the mesostructured samples with high quality. This following particular procedure was chosen because it was representative of TEOS-based xerogels reported in the literature [18,22–24,33,36,38,49–51]. A pre-hydrolyzed solution contains TEOS, ethanol, deionized water, and HCl ($1{:}3{:}5 \times 10^{-5}{:}1$, molar ratio) was first prepared by refluxing at 90 °C for 1 h to form the stock solution [50]. A little amount, 2 mL tetrahydrofuran, was added into the pre-hydrolyzed solution in order to solubilize the phen-Si in the sol more efficiently without disturbing the formation of the mesostructure of the final silicate products [49–51]. The sol was stirred for 15 min and then aged at room temperature for another 15 min, followed by an addition of surfactant (CTAB) solution in EtOH. To this sol was then added the second coupling agent phen-Si (molar ratio of phen-Si to final SiO_2 is 0.027) [51] and an additional amount of water and HCl to increase the concentration of HCl to 7.34 mM. The final molar ratio of constituents was: TEOS/EtOH/H_2O/HCl/CTAB = 1:22:5:0.004:0.14. Finally, $Ru(bpy)_2Cl_2 \cdot 2H_2O$ was added to the sol and the concentration of the $Ru(bpy)_2^{2+}$ complex in the sol was 5×10^{-3} M with respect to the final precursor solution. The sol was refluxed for 10 min in a nitrogen atmosphere until the sol color turned to transparent reddish-orange.

Transparent films were constructed by pippetting 100 μL of the final sol onto 2.5 cm × 2.5 cm sodalime silicate glass slides and spin-coating for 30 s at 3000 rpm. Each slide was first cleaned by soaking in 1 M NaOH for 30 min, washed ten times with deionized water and EtOH, and dried under ambient conditions. The quartz wafers with a thickness of 1 mm used for UV-vis electronic absorption spectra measurements were cleaned with 30% H_2O_2 and concentrated sulfuric acid (3:7 by volume) at 100 °C for 30 min and washed ten times with deionized water. The as-synthesized film was kept in the dark at ambient conditions (ca. 25 °C) for at least two weeks before any measurement. Adhesion to the substrate was found to be excellent. The residual sol was subsequently transferred into a covered cuvette with a few small pores in its cap and kept at 50 °C for 8–14 days to accomplish their gelation; in the end, a crack-free silica monolith was obtained. Samples were prepared in triplicate in order to investigate the batch-to-batch reproducibility.

It should be noted that sufficient aging time is necessary because insufficient ageing time yields a weak network that does not possess the dimensional stability to withstand the increasing compressive stress during the solvent-evaporation process [66], and causes macrocracks in the early drying stage at relatively high temperatures. Also, the rigid silica network formed after enough aging time is favorable to keep the highly ordered mesostructure, and too short an aging time would result in a disordered mesostructure. The result of our present work revealed that two weeks at 50 °C is long enough for the sol to yield an ordered mesostructure. The CTAB surfactant was removed by acid/solvent extraction, using a 1 M HCl solution in EtOH. The xerogel powders were refluxed for 12 h, then filtered and washed with EtOH to remove the HCl. The isolated product was vacuum-dried at 100 °C for 12 h. The surfactant extraction of the thin film was performed using the same method. The extracted films were washed with ethanol and then dried in vacuo at 50 °C for 1 h. For comparison, samples without surfactant were prepared under the same conditions. At the same time, in order to carry out the comparative studies of the covalently grafted and conventional physically incorporated $[Ru(bpy)_2phen]Cl_2$ complexes into the silicates for oxygen sensors, the samples replacing phen-Si for phen were prepared under the same conditions.

Instruments and Measurements: The IR absorption spectra were measured in the range 400–4500 cm^{-1} using an FT-IR spectrophotometer (Model Bruker Vertex 70 FTIR) with a resolution of ±4 cm^{-1} using the KBr pellet technique. The UV-vis electronic absorption measurements were performed with a Shimadzu UV-3000 spectrophotometer. Films spin-coated on quartz wafers were used for UV-vis electronic absorption spectra measurements. ^1H and ^{13}C NMR spectra were recorded on a Bruker AC 400 spectrometer. Elemental analyses of carbon, hydrogen, and nitrogen were carried out on a 240 Perkin–Elmer analyzer. The thickness measurements of the spin-coated films were performed using a variable-angle spectroscopic ellipsometer (Model 601BAM/I-Elli2000, Germanic NFT). The refractive index and thickness were calculated from the simulation parameters based on the Cauchy model. The profilometry experiments showed that the as-deposited film using the above-mentioned procedure was ca. 722.1 ± 0.2 nm. SAXRD patterns were recorded on a Philips PW 1710 diffractometer using Cu Kα_1 ($\lambda = 0.15405$ nm) radiation at a 0.02° (2θ) scanning step. The luminescent spectra of dried thin films and bulk xerogels were recorded in an aerated environment using a Hitachi-4500 fluorescence spectrophotometer.

The sensitivity properties of our present oxygen sensors were discussed based on the luminescence intensity quenching instead of the excited-state lifetime because it is hard to obtain the precise excited-state lifetime value with a conventional flashlamp-based time-correlated photon counting system. Optical oxygen sensors based on luminescence intensity in the sol–gel films and xerogel powders were characterized using the same Hitachi F-4500 fluorescence spectrophotometer. The emission spectra of different samples were obtained under excitation by the peak of the visible MLCT transition, and the excitation spectra were monitored at their maximum emission.

For the Stern–Volmer plot measurements, oxygen and nitrogen were mixed at different concentrations via gas-flow controllers and passed directly to the sealed gas chamber. We typically allowed 1 min between changes in the N_2/O_2 concentrations to ensure that a new equilibrium point had been established. Equilibrium was evident when the luminescence intensity remained constant (±2%). The sensor-response curve was obtained using the same method.

The time-resolved intensity decay measurements were carried out on the bulk xerogels using a Nd:YAG (neodymium yttrium aluminum garnet) laser system (Spectra Physics). The line width, repetition frequency, and pulse duration of the laser light were 1 cm^{-1}, 10 Hz, and 10 ns, respectively. Owing to the interference from the excitation source, geometrical considerations resulted in a sample orientation of

90°, to remove reflected and scattered excitation from entering the detector. A glass filter allowing light of wavelength >550 nm was placed between the sample and the monochromator to eliminate stray room and pump light. N_2 and O_2 gas was delivered to the sealed gas chamber in exactly the same manner as described above for the Stern–Volmer plot measurements. The maximum emission was set at 588 nm and the luminescence generated was detected using a photomultiplier. The signal was relayed through a 50 Ω termination plug that was passed into a digital phosphor oscilloscope (Tektronix, Beaverton, Oregon, US; Model TDS 3052) that was used to resolve the lifetime decay curves. All measured lifetimes presented were averaged 2400 times. The electronically excited-state decay time profiles were subsequently stored and analyzed using Origin 7.5. All measurements were performed at ambient temperature (23±5 °C).

Received: October 22, 2005
Final version: March 16, 2006
Published online: August 8, 2006

[1] L. C. Clark, Jr., *Trans. -Am. Soc. Artif. Intern. Organs* **1956**, *2*, 41.
[2] I. Bergman, *Nature* **1968**, *218*, 396.
[3] J. I. Perterson, R. V. Fitzgerald, D. K. Buckhold, *Anal. Chem.* **1984**, *56*, 62.
[4] J. R. Bacon, J. N. Demas, *Anal. Chem.* **1987**, *59*, 2780.
[5] P. Y. F. Li, R. Narayanaswamy, *Analyst* **1989**, *114*, 1191.
[6] E. R. Carraway, J. N. Demas, B. A. DeGraff, J. R. Bacon, *Anal. Chem.* **1991**, *63*, 337.
[7] D. B. Papkovsky, J. Olah, I. V. Troyanovsky, N. A. Sadovsky, V. D. Rumyantseva, A. F. Mironov, A. I. Yaropolov, A. P. Savitsky, *Biosens. Bioelectron.* **1992**, *7*, 199.
[8] X. Li, F. Ruan, K. Wong, *Analyst* **1993**, *118*, 289.
[9] W. W. S. Lee, K. Y. Wong, X. M. Li, *Anal. Chem.* **1993**, *65*, 255.
[10] I. Klimant, P. Belser, O. S. Wolfbeis, *Talanta* **1994**, *41*, 985.
[11] W. Xu, R. C. McDonough, B. Langsdorf, J. N. Demas, B. A. DeGraff, *Anal. Chem.* **1994**, *66*, 4133.
[12] Z. Rosenzweig, R. Kopelman, *Anal. Chem.* **1995**, *67*, 2650.
[13] T. Ishiji, M. Kaneko, *Analyst* **1995**, *120*, 1633.
[14] I. Klimant, O. S. Wolfbeis, *Anal. Chem.* **1995**, *67*, 3160.
[15] D. B. Papkovsky, G. V. Ponomarev, W. Trettnak, P. O'Leary, *Anal. Chem.* **1995**, *67*, 4112.
[16] J. N. Demas, B. A. DeGraff, W. Xu, *Anal. Chem.* **1995**, *67*, 1377.
[17] W. Xu, K. A. Kneas, J. N. Demas, B. A. DeGraff, *Anal. Chem.* **1996**, *68*, 2605.
[18] R. A. Dunbar, J. D. Jordan, F. V. Bright, *Anal. Chem.* **1996**, *68*, 604.
[19] A. Mills, M. Thomas, *Analyst* **1997**, *122*, 63.
[20] F. Alava-Moreno, M. J. Valencia-Gonzalez, A. Sanz-Medel, M. E. Díaz-García, *Analyst* **1997**, *122*, 807.
[21] A. Mills, A. Lepre, B. R. C. Theobald, E. Slade, B. A. Murrer, *Anal. Chem.* **1997**, *69*, 2842.
[22] M. T. Murtagh, M. R. Shahriari, M. Krihak, *Chem. Mater.* **1998**, *10*, 3862.
[23] C. McDonagh, B. D. MacCraith, A. K. McEvoy, *Anal. Chem.* **1998**, *70*, 45.
[24] Y. Tang, E. C. Tehan, Z. Tao, F. V. Bright, *Anal. Chem.* **2003**, *75*, 2407.
[25] M. F. Choi, D. Xiao, *Analyst* **1999**, *124*, 695.
[26] Y. G. Ma, T. C. Cheung, C. M. Che, J. C. Shen, *Thin Solid Films* **1998**, *333*, 224.
[27] C. McDonagh, P. Bowe, K. Mongey, B. D. MacCraith, *J. Non-Cryst. Solids* **2002**, *306*, 138.
[28] C. Malins, S. Fanni, H. G. Glever, J. G. Vos, B. D. MacCraith, *Anal. Commun.* **1999**, *36*, 3.
[29] A. K. McEvoy, C. M. McDonagh, B. D. MacCraith, *Analyst* **1996**, *121*, 785.
[30] S. K. Lee, I. Okura, *Analyst* **1997**, *122*, 81.
[31] M. M. F. Choi, D. Xiao, *Anal. Chim. Acta* **2000**, *403*, 57.
[32] X. Chen, Z. Zhong, Z. Lia, Y. Jiang, X. Wang, K. Wong, *Sens. Actuators B* **2002**, *87*, 233.
[33] Z. J. Fuller, W. D. Bare, K. A. Kneas, W. Y. Xu, J. N. Demas, B. A. DeGraff, *Anal. Chem.* **2003**, *75*, 2670.
[34] S. Draxler, M. E. Lippitsch, I. Klimant, H. Kraus, O. S. Wolfbeis, *J. Phys. Chem.* **1995**, *99*, 3162.
[35] B. D. MacCraith, C. M. McDonagh, G. O'Keeffe, E. T. Keyes, J. G. Vos, B. O'Kelly, J. F. McGlip, *Analyst* **1993**, *118*, 385.
[36] K. F. Mongey, J. G. Vos, B. D. MacCraith, C. M. McDonagh, C. Coates, J. J. McGarvey, *J. Mater. Chem.* **1997**, *7*, 1473.
[37] M. K. Krihak, M. R. Shahriari, *Electron. Lett.* **1996**, *32*, 240.
[38] P. Innocenzi, H. Kozuka, T. Yoko, *J. Phys. Chem. B* **1997**, *101*, 2285.
[39] H. Xu, J. W. Aylott, R. Kopelman, T. J. Miller, M. A. Philbert, *Anal. Chem.* **2001**, *73*, 4124.
[40] L. Sacksteder, J. N. Demas, B. A. DeGraff, *Anal. Chem.* **1993**, *65*, 3480.
[41] D. Dong, S. Jiang, Y. Men, X. Ji, B. Jiang, *Adv. Mater.* **2000**, *12*, 646.
[42] H. R. Li, J. Lin, H. J. Zhang, H. C. Li, L. S. Fu, Q. G. Meng, *Chem. Commun.* **2001**, 1212.
[43] A. C. Franville, D. Zambon, R. Mahiou, Y. Troin, *Chem. Mater.* **2000**, *12*, 428.
[44] A. C. Franville, R. Mahiou, D. Zambon, J. C. Cousseins, *Solid State Sci.* **2001**, *3*, 211.
[45] A. C. Franville, D. Zambon, R. Mahiou, S. Chou, Y. Troin, J. C. Cousseins, *J. Alloys Compd.* **1998**, *275–277*, 831.
[46] R. J. P. Corriu, F. Embert, Y. Guari, A. Mehdi, C. Reyé, *Chem. Commun.* **2001**, 1116.
[47] H. R. Li, J. Lin, H. J. Zhang, L. S. Fu, Q. G. Meng, S. B. Wang, *Chem. Mater.* **2002**, *14*, 3651.
[48] Z. Hua, J. Shi, L. Wang, W. Zhang, *J. Non-Cryst. Solids* **2001**, *292*, 177.
[49] H. Li, L. Fu, F. Liu, S. Wang, H. Zhang, *New J. Chem.* **2002**, *26*, 674.
[50] F. Cagnol, D. Grosso, G. J. A. A. Soler-Illia, E. L. Crepaldi, F. Babonneau, H. Amenitsch, C. Sanchez, *J. Mater. Chem.* **2003**, *13*, 61.
[51] L. Nicole, C. Boissière, D. Grosso, P. Hesemann, J. Moreau, C. Sanchez, *Chem. Commun.* **2004**, 2312.
[52] C. Peng, H. Zhang, J. Yu, Q. Meng, L. Fu, H. Li, L. Sun, X. Guo, *J. Phys. Chem. B* **2005**, *109*, 15278.
[53] M. Wrighton, D. L. Morse, *J. Am. Chem. Soc.* **1974**, *96*, 998.
[54] F. N. Castellano, T. A. Heimer, M. T. Tandhasetti, G. J. Meyer, *Chem. Mater.* **1994**, *6*, 1041.
[55] P. J. Giordano, M. S. Wrighton, *J. Am. Chem. Soc.* **1979**, *101*, 2888.
[56] C. E. Fowler, B. Lebeau, S. Mann, *Chem. Commun.* **1998**, 1825.
[57] V. W. W. Yam, B. Li, N. Zhu, *Adv. Mater.* **2002**, *14*, 719.
[58] B. H. Han, I. Manners, M. A. Winnik, *Chem. Mater.* **2005**, *17*, 3160.
[59] K. Matsui, F. Momose, *Chem. Mater.* **1997**, *9*, 2588.
[60] A. Mills, Q. Chang, *Analyst* **1992**, *117*, 1461.
[61] A. Mills, A. Lepre, *Anal. Chem.* **1997**, *69*, 4653.
[62] G. Sprintschnik, H. W. Sprintschnik, P. P. Kirsch, D. G. Whitten, *J. Am. Chem. Soc.* **1977**, *99*, 4947.
[63] K. Binnemans, P. Lenaerts, K. Driesen, C. Görller-Walrand, *J. Mater. Chem.* **2004**, *14*, 191.
[64] J. P. Lecomte, A. K. D. Mesmaeker, *J. Chem. Soc. Faraday Trans.* **1993**, *89*, 3261.
[65] G. M. Kloster, C. M. Taylor, S. P. Watton, *Inorg. Chem.* **1999**, *38*, 3954.
[66] L. L. Hench, J. K. West, *Chem. Rev.* **1990**, *90*, 33.